UC Davis
UC Davis Previously Published Works

Title

1D Lignin-Based Solid Acid Catalysts for Cellulose Hydrolysis to Glucose and Nanocellulose

Permalink

https://escholarship.org/uc/item/1t4608p8

Journal

ACS Sustainable Chemistry & Engineering, 3(10)

ISSN

2168-0485

Authors

Hu, Sixiao
Jiang, Feng
Hsieh, You-Lo

Publication Date

2015-10-05

DOI

10.1021/acssuschemeng.5b00780

Peer reviewed

1D Lignin-Based Solid Acid Catalysts for Cellulose Hydrolysis to Glucose and Nanocellulose

Sixiao Hu, Feng Jiang, and You-Lo Hsieh*

Fiber and Polymer Science, University of California-Davis, One Shields Avenue, Davis, California 95616, United States

Ⓢ Supporting Information

ABSTRACT: One-dimensional (1D) solid acid catalysts have been synthesized from lignin-based activated carbon fibers via sulfonation and hydrothermal treatment to be mesoporous and contain 0.56 mmol/g sulfonic and 0.88 mmol/g total acid for direct hydrolysis of highly crystalline rice straw cellulose (CrI = 72.2%). Under optimal hydrothermal conditions of 150 °C and 5 atm, 69.8% of cellulose was hydrolyzed in three consecutive runs, yielding 64% glucose at 91.7 selectivity as well as 8.1% cellulose nanofibrils (2.1 nm thick, 3.1 nm wide, and up to 1 μm long). These 1D acid catalysts could be used repetitively to hydrolyze the remaining cellulose as well as be easily separated from products for hydrolysis of additional cellulose. In essence, complete valorization of rice straw cellulose has been demonstrated by direct hydrolysis with these 1D acid catalysts to superior glucose selectivity while generating high value cellulose nanofibrils.

KEYWORDS: Solid acid catalysts, Mesoporous, Activated carbon fibers, Hydrolysis, Glucose, Cellulose nanofibrils
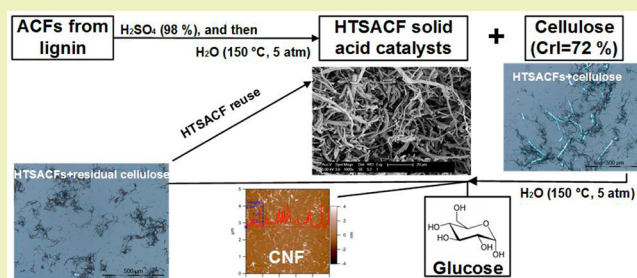
INTRODUCTION

Heterogeneous solid acid catalysts are particularly suited for large-scale industrial operations due to their many advantages over homogeneous liquid phase catalysts. Heterogeneous solid acid catalysts are noncorrosive and safe and can function more efficiently under continuous flow than the typical batch operations of homogeneous liquid acid catalysts.[1] In solid acid catalysis, the reactants can be activated directly by protons generated from the acid sites or via hydrogen spillover from other active phases in the system.[2] The products could be easily separated to allow recovery and reuse of the solid catalysts. Various solid acid catalysts, such as zeolite,[3–6] silica,[7–12] hydrous zirconia,[12] nafion[13–15] and carbons,[16–19] have been developed for common chemical reactions, including esterification,[3,12,16] alcohol dehydration,[7,13] and hydrolysis.[18,19]

Solid catalysts have also been reported in the hydrolysis of cellulose for biofuel production, including nafion,[15] zeolite,[20] Fe_3O_4 magnetic nanoparticles bearing mesoporous silica,[21] nano Zn-Ca-Fe oxide,[22] as well as a wide range of cellulose chars and activated carbon particulates.[18,19,23–29] Among them, carbon solid acid catalysts have exhibited particularly high activity because of their high acid densities and strong interactions with the β-1,4-glycosidic bonds in cellulose.[28] An exceptional 74% glucose yield was achieved under hydrothermal conditions using sulfonated ordered mesoporous carbon derived from a silica template.[18] However, either ball milling[18,26,29] or ionic liquid dissolution of cellulose[27] was necessary to enhance contact or diffusion to destruct the crystalline structure of cellulose. To overcome the accessibility issue, smaller Zn-Ca-Fe oxide nanoparticle catalysts have been

shown to significantly increase the hydrolysis of crystalline cellulose into glucose and oligosaccharides.[22] Separation of zero-dimensional nanocatalysts from the hydrolysate products is, however, difficult. Therefore, solid acid catalysts with high acid densities and yet geometries that allow easy separation for reuse would be of significant interest. Furthermore, solid acid hydrolysis of cellulose should generate nanocellulose, but this has only been reported on solid cationic exchange polystyrene resin beads (NKC-9 with 4.7 mmol/g acid density).[30]

This study aimed to synthesize one-dimensional (1D) solid acid catalysts for direct hydrolysis of crystalline cellulose for simultaneous production of sugars and high valued nanocellulose. The 1D solid acid catalysts were prepared from sulfonation of submicron-sized activated carbon fibers (ACFs) using concentrated sulfuric acid. The ultrafine ACFs were electrospun from lignin and simultaneously carbonized and activated at 900 °C to high specific surface (1400 m²/g) and pore volume (0.7 cm³/g).[31] The solid acid catalysts from lignin-based ACFs have several advantages and desired attributes over other solid acid catalysts for hydrolysis of crystalline cellulose. Lignin, an abundant and underutilized biomass fraction, is an excellent carbon precursor, and lignin chars are less recalcitrant than rigid graphitic carbons, such as carbon nanotubes,[18] to be readily sulfonated by concentrated sulfuric acid, a much safer alternative than the commonly used fuming sulfuric acid for sulfonation of graphitic carbons. These 1D solid acid catalysts

can be directly mixed with untreated semicrystalline cellulose. ACFs, with the high aspect ratio, submicron diameters, and porous structures are expected to be in more intimate contact with cellulose, affording shorter access to the active sites and better interconnected diffusive pathways for rapid and efficient hydrolysis while minimizing deactivation of the catalysts. The continuous fibrous form of the solid acid catalysts can be easily separated from the soluble products via simple filtration for repetitive use.

■ EXPERIMENTAL SECTION

Materials. Pure cellulose was isolated from rice straw (Calrose variety) by extraction with 2:1 v/v toluene/ethanol and subsequent dissolution of lignin and hemicellulose/silica with acidified NaClO$_2$ (1.4 wt %, 70 °C, 5 h) and alkaline KOH (5 wt %) at 90 °C for 2 h resulting in 36% yield and 72.2% crystallinity.[32,33] Poly(ethylene oxide) (PEO) (M_w = 600 kDa), alkali lignin (low sulfonate) (AL$_{ls}$) (M_w = 60 kDa, spruce origin) were acquired from Sigma-Aldrich (USA), sodium hydroxide (anhydrous NaOH pallets, A.C.S. grade, 85 wt % minimum purity), aqueous NaOH (1N), sulfuric acid (95−98 wt % purity), dinitrosalicylic acid (98 wt % purity), sodium sulfite anhydrous (98 wt % minimum purity), potassium sodium tartrate tetrahydrate (A.C.S. grade), and water (HPLC grade) were from Fisher Scientific (USA). All of the chemicals were used as received.

Synthesis of Solid Acid Catalysts. Both carbon fibers (CFs) and activated carbon fibers (ACFs) were synthesized according to a previously reported approach.[31] Briefly, aqueous 9:1 w/w AL$_{ls}$/PEO (10 wt % total concentration) mixtures without and with NaOH at a 1:2 w/w NaOH/lignin ratio were electrospun into CF and ACF precursor fibers, respectively. The precursor fibers were placed in a quartz tube (2 cm inner diameter) of an electric furnace (Mini-Mite, Lindberg/Blue), heated at 10 °C min^{-1} under flowing N$_2$ at 100 mL min^{-1} to 105 °C, held for 0.5 h to drive off moisture, and then to 600 (CFs) or 900 °C (CFs and ACFs), held for another 0.5 h, and finally cooled to ambient temperature under flowing N$_2$ at 100 mL min^{-1}. CFs and ACFs were then washed with deionized water repeatedly to remove residual alkali metals and other small hydrocarbon impurities followed by oven drying at 60 °C for 12 h.

Dried CFs and ACFs were sulfonated with concentrated sulfuric acid at 110 or 150 °C for 20 h (5 mg/mL solid/liquid ratio, 1 atm) to obtain sulfonated CF (SCFs) and ACFs (SACFs), respectively. SACFs were rinsed thoroughly with 70 °C water to remove residual sulfuric acid and then heated in water at 150 °C and 5 atm for 24 h using a 100 mL poly(tetrafluoroethylene) cylindrical reactor to obtain the hydrothermal-treated SACFs. Hydrothermal-treated SACFs sulfonated at 150 °C were further characterized and used in the hydrolysis of cellulose and were denoted as HTSACFs unless specified otherwise.

Hydrolysis of Cellulose. Solid HTSACFs catalyst (160 mg) and cellulose (40 mg) were dispersed in 32 mL of water in a 100 mL PTFE cylindrical reactor, hermetically sealed, and heated in 110, 130, and 150 °C oil baths for 24 h with corresponding pressures of 1.4, 2.8, and 5.0 atm, respectively. The catalysts and remaining cellulose were vacuum filtered (Whatman No. 1, dried, and weighed to 0.1 mg). The average mass of the remaining cellulose and the catalysts (m$_{cell+HTSACF}$) from five reactions were used to determine the extent of cellulose hydrolysis via eq 1. For repetitive hydrolysis, the dried HTSACF catalysts along with the remaining cellulose were redispersed to 32 mL of water and heated at 150 °C for a second and then a third time with drying and weighing in between to determine the extent of cellulose hydrolysis for each repetition. The filtrates were thoroughly dialyzed (12−14 kDa MWCO, Fisher brand) to exchange the sugars in the aqueous environment and retain nanocellulose in the dialysis membrane. The glucose produced was quantified by the colorimetric assay as described later. The nanocellulose yield was determined gravimetrically by weighing dried nanocellulose and reported as a percentage of the original cellulose.

$$\text{cellulose hydrolysis (wt \%)} = \frac{m_{cell+HTSACF} - 160}{40} \times 100\% \quad (1)$$

Analytical Methods. The chemical structures of ACFs, SACFs, and HTSACFs were examined by Fourier transform infrared spectroscopy (FTIR) (Nicolet 6700, Thermo Scientific), and their morphologies were characterized by scanning electron microscope (SEM) (FEI-XL 30, FEI) and atomic compositions by energy-dispersive X-ray spectroscopy (EDX) adjunct to the SEM. All samples were washed thoroughly with deionized water and dried at 60 °C for at least 12 h before characterization. All FTIR spectra were collected from samples pressed with anhydrous KBr powders into pellets. All samples were sputter coated with gold for 1 min and imaged by SEM, and noncoated samples were analyzed by EDX under a working voltage of 5 kV. The acid density of the catalysts was analyzed via conductometric titration using a pH/conductivity meter (510, OAKTON). For each titration, 10 mg of the acid catalysts were dispersed in 15 mL of water, and 0.02 N NaOH was added to neutralize the acids. The surface acid density (σ, in mmol/g of the solid acid catalyst) was calculated from eq 2, where c is the NaOH concentration (in N), m is the mass of the catalyst (in g), and V is the volume of NaOH (in mL) used to neutralize the sulfonic acid and total acids on the catalysts.

$$\sigma = \frac{cV}{m} \quad (2)$$

For surface area and pore characterization, the ACFs, SACFs, and HTSACFs were dried at 50 °C for 48 h and then measured at 77 K by a nitrogen adsorption−desorption analyzer (ASAP 2020, Micrometics). The single point total pore volume was estimated from nitrogen adsorption at a relative pressure P/P_o close to 1. The Brunauer−Emmett−Teller (BET) surface area was calculated from the isotherm in the BET linear region where relative pressure P/P_o ranged from 0.05 to 0.3. The mesopore surface area was derived from the adsorption branch whereas pore and neck size distributions were derived from both adsorption and desorption branches of the isotherm using the Barret−Joyner−Halenda (BJH) method. To derive micropore characteristics from the adsorption−desorption isotherm with incomplete data below 0.05 P/P_o relative pressure, micropore surface area and pore hydraulic diameter distributions from 0.7 to 1.6 nm were derived from a t-plot using the Mikhail, Brunauer, and Bodor MP method[34] and the Harkins and Jura equation.[35] Micropore volume (V_{mp}) was derived from the tangent line of a contiguous range of the t-plot using the surface area of the filled pores via eq 3

$$V_{mp} = \frac{(S_n - S_{n+1})(t_n + t_{n-1})}{2} \times 15.47 \quad (3)$$

where S_n and t_n are the surface area derived from the slope of the tangent and the thickness of the adsorbed layer at the n point in the t-plot, respectively, and 15.47 was the constant for converting gas volume to liquid volume at STP.

The mixed HTSACF catalysts/cellulose (4:1) before and after three consecutive reactions (32 mL of water and 150 °C) were sonicated in a water bath (Branson 2510) for 10 min and then visualized under a polarizing light microscope (PLM, LEICA DM 2500). The nano-cellulose separated from the catalyst by dialysis was diluted 10×, of which 10 μL was deposited onto a freshly cleaved mica surface, air-dried, and scanned using an atomic force microscope (AFM, MFP 3D, Asylum Research) under ambient air conditions in the tapping mode with OMCL-AC160TS standard silicon probes at 1 Hz scan rate and 512 × 512 pixel resolution. The height image and profile were processed with Igor Pro 6.21 loaded with MFP3D 090909 + 1409, and the average thickness was determined from ~100 individual nanocellulose. Using a transmission electron microscope (TEM), a diluted nanocellulose suspension (5 μL) was deposited onto glow-discharged carbon-coated grids (300 mesh copper, Formvar-carbon, Ted Pella Incorporated, Redding, CA) with excess liquid being removed by blotting with filter paper after 10 min, negatively stained with 2 wt % uranyl acetate solution for 5 min, and observed using a Philip CM12 TEM operated at 100 kV accelerating voltage. The width

of the nanocellulose was measured from ~100 individual nanofibrils using an image analyzer (ImageJ, NIH, USA).

The water-soluble hydrolysates (10 μL) were injected into a 0.32 mm × 100 mm Hypercarb column, and the compositions were analyzed by LC−MS (Thermo Scientific, USA). A standard reverse-phase gradient utilizing 5 mM ammonium formate as solvent "A" and acetonitrile as solvent "B" was run at a 25 μL/min flow rate for 12 min. The eluent was monitored for negative ions by an orbitrap XL (Thermo Scientific, USA) operated in the centroid mode at 4.5 kV spray voltage, 275 °C capillary temperature, and 20 sheath gas setting. Spectral data were acquired at a 30,000 fwhm resolution setting with the lockmass feature, which has a typical mass accuracy of <2 ppm. The glucose concentration was derived from the colorimetric assay.[36] Briefly, 100 mL of 1 wt % dinitrosalicylic acid reagent (DNS) solution was prepared by mixing 1 g of dinitrosalicylic acid, 1 g of sodium hydroxide, and 50 mg of sodium sulfite. Then, 1.5 mL of DNS solution and 1.5 mL of hydrolysate were mixed and then heated at 90 °C for 10 min to develop the red-orange color, which was stabilized by subsequently adding 1 mL of 40 wt % potassium sodium tartrate solution. Upon cooling to ambient temperature, the UV−vis absorbance of the stabilized solution was measured (Evolution 600, Thermo Scientific) at 575 nm. Their sugar concentrations were derived from the standard calibration using glucose solutions in 0.125 to 1.25 mg/mL concentrations (Figure S1). The glucose yield and selectivity were calculated based on the original cellulose (40 mg) via eqs 4 and 5, respectively, where C_g is the glucose concentration (mg/mL) determined by colorimetric titration and V_g is the volume of the hydrolysate (mL).

$$\text{glucose yield (\%)} = \frac{C_g \times V_g}{40} \times 100\% \quad (4)$$

$$\text{glucose selectivity (\%)} = \frac{\text{glucose yield}}{\text{cellulose hydrolysis}} \times 100\% \quad (5)$$

■ RESULTS AND DISCUSSION

Acid Density and Chemical Structures of Solid Acid Catalysts. Sulfonated carbon fibers (SCFs) and sulfonated activated carbon fibers (SACFs) were prepared under two carbonization (T_c = 600 or 900 °C) and sulfonation (T_s = 110 or 150 °C) temperatures (Table 1). The SACFs carbonized at

Table 1. Sulfonic and Total Acid Density (mmol/g) of Sulfonated Carbon Fibers (SCFs) and Sulfonated Activated Carbon Fibers (SACFs) Prepared at the Prescribed Carbonization (T_c) and Sulfonation (T_s) Temperatures

		T_s = 110 °C		T_s = 150 °C	
sample	T_c (°C)	sulfonic acid	total acid	sulfonic acid	total acid
SCF	600	1.2	1.4	1.4	1.9
SCF	900	0.3	0.41	0.52	0.68
SACF	900	0.7	1.11	1.62	2.43
HTSACF	900	0.31	0.48	0.56	0.88

900 °C were also hydrothermal-treated (150 °C, 5 atm, 24 h) to obtain HTSACFs. The acid densities were determined by conductometric titration where conductivity typically decreased sharply from neutralization of sulfonic acid groups, then stayed constant as the weaker carboxylic acid was consumed, and finally increased after all acid sites were neutralized with NaOH addition (Figure S2). In all titration curves, sulfonic acid was shown to be dominant with much lower extents of carboxylic acid groups. Although sulfonic acid is expected from the sulfonation reaction, carboxylic acid groups are likely from oxidation of the reductive hydroxyl groups during prolonged sulfonation.

Both sulfonic and total acid densities were higher for SCFs carbonized at the lower 600 °C T_c and for all fibers sulfonated at the higher 150 °C T_s (Table 1). SCFs carbonized at the higher 900 °C had approximately 1/4 to 1/3 of the respective sulfonic and total acid densities, i.e., 0.3 and 0.41 mmol/g at T_s = 110 °C and 0.52 and 0.68 mmol/g at T_s = 150 °C, respectively, of those carbonized at 600 °C. Sulfonation of ACFs (T_c = 900 °C) at the respective T_s of 110 and 150 °C on SACFs, on the other hand, doubled and tripled the sulfonic and total acid quantities relative to the corresponding SCFs. Although the more rigid carbon structures produced at the higher carbonization temperature of 900 °C are more difficult to be sulfonated, hence lower acid densities, higher specific surface ACF could only be produced at 900 °C. The greater sulfonation effects on ACFs are due to their higher internal surfaces as well as the carbon microstructure defects introduced by alkali hydroxide activation.[37] Most significantly, the higher sulfonation temperature produced increases in sulfonic and total acids on the activated SACFs that were more pronounced than on the SCFs. Overall, the SACFs carbonized at higher 900 °C still had a much higher acid density than SCFs carbonized at lower 600 °C and therefore were hydrothermally treated to prepare stable solid acid catalysts. Following hydrothermal washing (150 °C, 5 atm, 24 h), the sulfonic and total acid densities of HTSACFs sulfonated at 110 and 150 °C declined significantly by 55% (0.31 and 0.48 mmol/g) and 65% (0.56 mmol/g and 0.88 mmol/g), whereas their mass decreased to lesser degrees of 5 and 9%, respectively. The substantial losses of sulfonic and total acids coupled with some mass losses from hydrothermal washing suggest that sulfonation of the pore surfaces may have led to fragmentation and solubilization of small hydrocarbons. Both surface acid densities and catalyst mass remained unchanged following a second hydrothermal washing, showing no further leaching. That these acid sites remain stable under the hydrothermal catalysis condition is a critical attribute for HTSACF solid acid catalysts to be effective in repetitive use. HTSACFs sulfonated at 150 °C with higher sulfonic (0.56 mmol/g) and acid (0.88 mmol/g) densities was used as the solid acid catalyst for the hydrolysis of cellulose to be described later.

The presence of carboxylic and sulfonic acid groups on ACFs, SACFs, and HTSACFs was further confirmed by FTIR and EDX. Both FTIR spectra of SACFs and HTSACFs showed a C═O peak at 1720 cm^{-1} but no evidence of the C−OH peak at 1630 cm^{-1} (Figure 1a), indicating complete oxidation of C−OH to carbonyl and carboxylic acid by the concentrated sulfuric acid. Aromatic skeletal stretching at 1580 cm^{-1}, expected from the polycyclic aromatic structures in all three activated carbons, was also clearly present. In addition, EDX showed the O content to be tripled from 4.4 wt % in ACFs to 12.7 wt % in SACFs in which 2.8 wt % of S was also detected (Figure 1b). The hydrothermal treatment significantly lowered the respective O and S contents in SACFs to 7.3 and 0.9 wt % in HTSACFs. Such elemental composition changes were consistent with the decreases in sulfonic and total acid densities presented previously and attributed to the dissolution of the highly oxidized and sulfonated hydrocarbons from the hydrothermal treatment.

Morphologies and Porous Structures of the Solid Acid Catalysts. ACFs were 500 nm to 2 μm wide and most were over 100 μm long (Figure 2a and b). Sulfonation caused SACFs to fragment into a few tens of micrometers in length. This obvious length reduction is attributed to the extreme
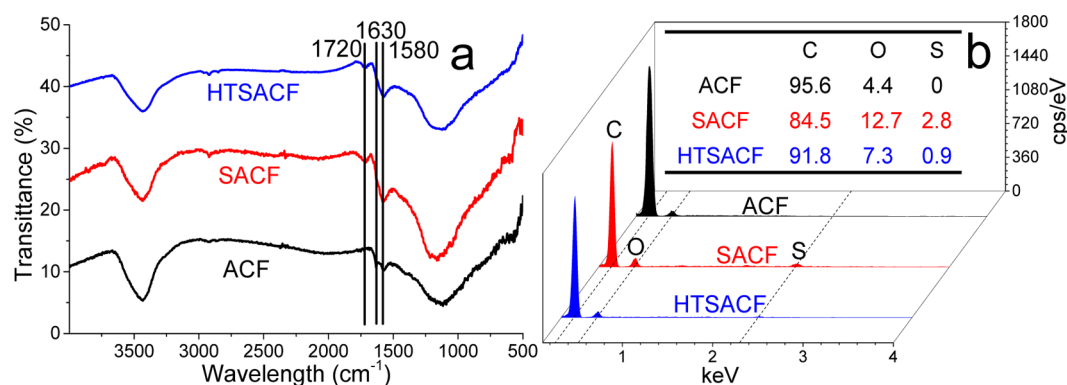
Figure 1. (a) FTIR and (b) EDX of ACF, SACF, and HTSACF. Inset in (b): elemental composition (wt %).
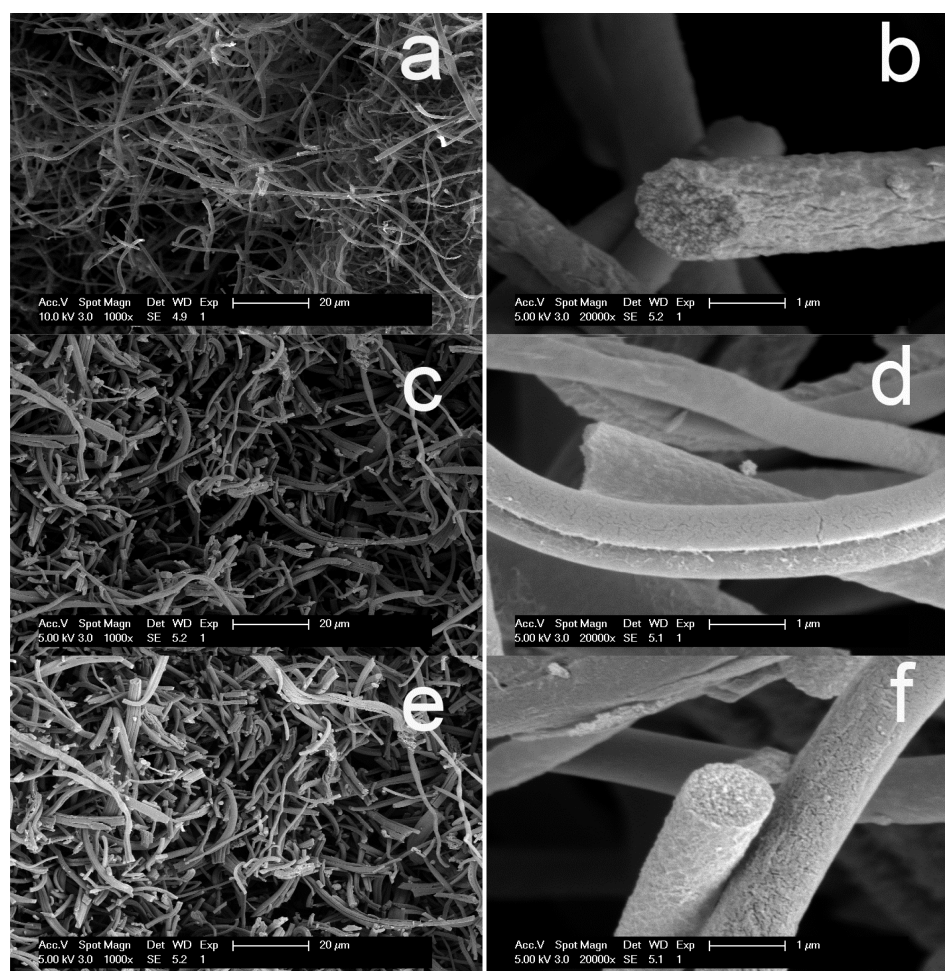

Figure 2. SEM of (a,b) ACFs, (c,d) SACFs, and (e,f) HTSACFs.

oxidation in concentrated sulfuric acid and the mechanical forces from magnetic agitation (Figure 2c and d). The hydrothermally washed HTSACFs remained similarly fragmented but showed no further morphological changes (Figure 2e and f). All three fibers, i.e., ACFs, SACFs, and HTSACFs, appeared similarly porous with surface macropores in the tens of nanometers range (Figure 2b, d, and f).

The porous structures of ACFs, SACFs, and HTSACFs were further analyzed by BET nitrogen adsorption to all exhibit type IV adsorption−desorption isotherms (Figure 3a) typical of microporous and mesoporous materials. Each showed a step-down at 0.45 relative pressure in the desorption isotherm

(Figure 3a) and an artificial peak at 4 nm (Figure 3b), suggesting an ink-bottle porous structure with a neck size smaller than 5 nm.[38,39] The sulfonation reaction slightly and hydrothermal treatment more prominently shifted the meso-pores to larger pore sizes and wider ranges (Figure 3b and c). Sulfonation slightly increased the mesopore (5−30 nm) surface area and volume from 407 m^2/g to 416 m^2/g and from 0.71 to 0.75 cm^3/g, respectively (Figure 3c), but significantly decreased micropore (0.5−0.8 nm) surface area and volume from 444 to 305 m^2/g and 0.18 to 0.13 cm^3/g, respectively (Figure 3d), resulting in a slight decrease in the total BET surface area (885 to 752 m^2/g) and pore volume (0.9 to 0.88 cm^3/g).
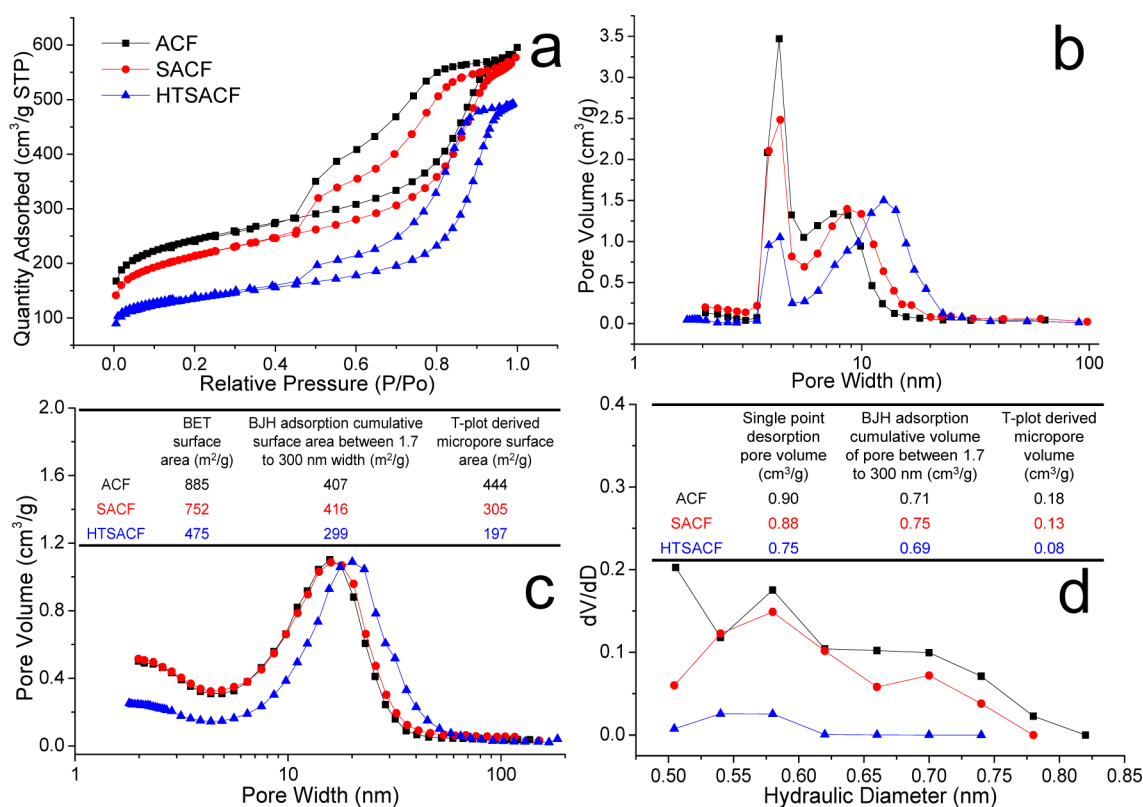
Figure 3. Nitrogen adsorption−desorption of ACFs, SACFs, and HTSACFs: (a) isotherm, (b) BJH neck size distribution from the isotherm desorption branch, (c) BJH pore/cavity width distribution from the isotherm adsorption branch, and (d) micropore hydraulic diameter distribution. Inset tables: (c) surface area, (d) pore volume.

Hydrothermal treatment reduced both BJH mesopore and t-plot-derived micropore surface areas to 299 and 197 m²/g and corresponding pore volumes to 0.69 and 0.08 cm³/g, respectively, suggesting ~90% of the pores were mesopores in the 5−50 nm range. Overall, the micropores were reduced by sulfonation and hydrothermal treatment consecutively, whereas the mesopores were reduced mainly by the latter. As both processes involved elevated temperatures, reduced micropores from sulfonation may be more due to chemical functionalization of the micropore surfaces, whereas reduced micropores and mesopores from hydrothermal treatment may be attributed to the loss of soluble hydrocarbons as well as collapse of both under high pressure. Therefore, the microporous and mesoporous ACFs became less microporous SACFs from sulfonation then to mesopore-dominated HTSACFs from the hydrothermal treatment.

Although the isotherms of all samples exhibited mainly H2 hysteresis, the transition to H1 hysteresis was observed from SACFs to HTSACFs in particular as the vertically parallel symmetry of the adsorption and desorption branches started to develop. This indicated that the pores became more isolated, possibly due to the collapse of the interconnecting micropores. However, such a decrease in microporosity should have minimal effects on the hydrolysis of oligosaccharides that are larger than 1 nm and not accessible to the micropores. These mesopores along with macropores observed on the fiber surfaces, conversely, are critical to the transport of oligosaccharides to the acid sites on the internal pores within the solid acid HTSACF catalysts, leading to more extensive hydrolysis. The more fragmented fibrous structure of the solid acid HTSACF catalysts were deemed beneficial to better mixing and contacts with the cellulose substrates, enhancing hydrolysis, whereas the surface macropores and internal mesopores could facilitate the transport of the hydrolysates in and out of the acid sites on the pore surfaces.

The Extent and Products of Cellulose Hydrolysis. The ability of HTSACF solid acid catalysts bearing 0.56 mmol/g sulfonic and 0.32 mmol/g carboxylic acid groups to hydrolyze semicrystalline (CrI = 72.2%) rice straw cellulose was evaluated under hydrothermal conditions at varying temperatures for 24 h. The extent of cellulose hydrolysis increased from 20.8 to 27.7 and 33.4% upon increasing the temperature from 110 to 130 and 150 °C at corresponding 1.4, 2.8, and 5.0 atm pressures, respectively (Table 2). Hydrolysis of cellulose by HTSACFs at 150 °C was repeated a second and third time, showing additional 32.3 and 33.1% of each residual cellulose, or 21.5 and 14.9% of the original cellulose, hydrolyzed in the respective repetitions. The extents of cellulose hydrolysis remained at

Table 2. Cellulose Hydrolysis and Yields of Glucose and CNF from HTSACF-Catalyzed Cellulose[a]

temperature (°C)	pressure (atm)	cellulose hydrolysis (%)	glucose (%)	glucose selectivity (%)	CNF (%)
110	1.4	20.8	19.1	91.8	NA
130	2.8	27.7	25.3	91.3	2.1
150 1st	5.0	33.4	29.9	89.5	2.3
2nd	5.0	21.5	20.2	91.2	2.5
3rd	5.0	14.9	13.9	91.7	3.3
cumulative		69.8	64		8.1

[a]All percentages based on original cellulose.

~33%, essentially constant among the three consecutive runs, indicating highly consistent catalytic performance and high stability of HTSACFs. The cumulative extent of hydrolysis was 69.8% from three repetitions, demonstrating the high efficiency of the HTSACF solid acid catalyst in directly hydrolyzing semicrystalline cellulose without pretreatment. Furthermore, additional cellulose could be added for continuing hydrolysis and reusing the HTSACF catalyst.

The optical microscope images of the cellulose and HTSACF mixtures under a cross polarizer clearly showed numerous submicron-wide HTSACF fibrous catalysts wrapping around the micrometer-wide cellulose fibers in the initial mixture before hydrolysis, whereas only trace amounts of cellulose fibers were observed among HTSACFs after three consecutive repetitions of hydrolysis (Figure 4). The highly efficient
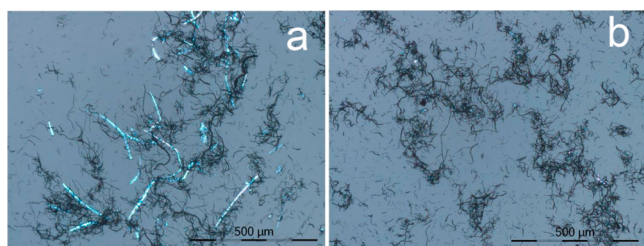

Figure 4. Optical microscope images of crystalline cellulose (light blue) and HTSACF catalyst mixture (black) under a cross polarizer (a) before and (b) after three consecutive hydrolyses.

hydrolysis of untreated semicrystalline cellulose was attributed to the affinity and close contact of the much finer and higher aspect ratio HTSACF fibers with the cellulose fibers.

It was thought that the hydronium ions from the solid acid catalysts could access and penetrate into cellulose structures when the large crystalline celluloses were wrapped by the much finer carbon fibers, similar to liquid acid, and exhibited high hydrolysis efficiency (Figure S3).

The LC of the hydrolysates from the hydrolysis reactions at 110, 130, and 150 °C all exhibited predominant peaks between 1.2 and 1.5 min (Figure S4). The mass spectrum all three eluents showed the same major peak with a mass of 225.06 m/z corresponding to glucose-formate ion. The minor peaks at 223, 224, 226, and 227 could be due to the isotopes. The absence of peaks associated with other oligosaccharides in LC-MS indicated glucose to be the only product of hydrolysis in all cases, a clear sign of high glucose selectivity. The yields of glucose determined by colorimetric analysis were 19.1, 25.3, and 29.9% at 110, 130, and 150 °C, respectively, and the

cumulative glucose yields at 150 °C were 29.9, 50.1, and 64% from the three consecutive hydrolyses. On the basis of the 20.8−69.8% extent of cellulose hydrolysis under all conditions studied, these glucose yield values showed that 89.5−91.7% of the cellulose was hydrolyzed into glucose. The ~90% glucose selectivity is excellent.

The high glucose selectivity of these solid acid HTSACF catalysts is clearly superior to those of a variety of recently reported solid catalysts (Table 3) from which other oligosaccharides, levulinic acid, and hydroxymethylfurfural byproducts were also reported. Another merit of these solid acid HTSACF catalysts is their ability to directly and efficiently hydrolyze highly crystalline and nonpretreated cellulose. Although CMK-SO$_3$H[18] and HY-zeolite[20] could hydrolyze 84−94% of cellulose, the cellulose used was ball-milled to be rendered amorphous. These HTSACF solid acid catalysts showed 300% higher extent of hydrolysis of untreated cellulose than nafion fibers,[15] 15% higher than mesoporous silica SBA15,[21] and even slightly higher than Zn-Ca-Fe oxide nanoparticles.[22] The glucose selectivity of the HTSACF catalyst was also 300% higher than commercially available activated carbons,[18] 15% higher than mesoporous carbons produced via a reverse mesoporous silica template,[18] and 11% higher than nafion fibers.[15] The excellent hydrolysis efficiency and glucose selectivity demonstrated the superior performance of the HTSACF catalyst in hydrolyzing crystalline cellulose over the solid catalysts reported to date.

In addition to the high glucose selectivity and efficiency, direct hydrolysis of crystalline cellulose by the HTSACF catalyst also produced nanocellulose that could be easily separated from glucose by dialysis. The yields of nanocellulose based on the starting cellulose were 2.3, 2.5, and 3.3% from three consecutive hydrolyses at 150 °C or a cumulative yield of 8.1% (Table 2). The nanocellulose after the first hydrolysis consisted primarily of long and flexible cellulose nanofibrils (CNFs) and a small amount of much shorter cellulose nanocrystals (CNCs) with lengths varying from 100 nm up to 1 μm (Figure 5a and c). The average nanocellulose thickness and width determined by AFM height (inset in Figure 5a) and TEM (Figure 5c) images were 2.1 ± 1.0 and 3.1 ± 0.7 nm, respectively (Figure 5b and d). The nanocellulose suspension from the first hydrolysis was dried at 50 °C to form self-standing films, showing iridescent colors, consistent with the presence of rodlike cellulose nanocrystals that could concentrate to form an ordered nematic liquid crystalline phase (Figure S5). Nanocellulose from the second and third hydrolysis also showed predominantly CNFs, with few CNCs, similar to those from the first hydrolysis (Figure S6a),

Table 3. Comparisons of Solid Acid Catalyzed Hydrolysis of Cellulose^a

catalyst	acid density (mmol/g)	pretreatment	solvent	temperature (°C)	cellulose hyrolysis (wt %)	glucose yield (wt %)	glucose selectivity (%)
HY-zeolite[20]	1.36	milled	[C$_4$mim]Cl/ H$_2$O	130	84.3	50	59.3
CMK-SO$_3$H[18]	2.39	milled	H$_2$O	150	94.4	74.5	78.9
activated carbon-SO$_3$H[18]	0.22	milled	H$_2$O	150	25.1	7.1	28.3
Fe$_3$O$_4$−SBA-SO$_3$H[21]	1.09	none	H$_2$O	150	n/a	26	n/a
Nafion SAC50[15]	n/a	none	H$_2$O	190	11	9	81.8
Zn-Ca-Fe oxide nanoparticles[22]	n/a	none	H$_2$O	150	n/a	29	n/a
HTSACFs (this work)	0.88	none	H$_2$O	150	33	29.9	91.7

^{a}Microcrystalline cellulose in all cited work; rice straw cellulose in this work.
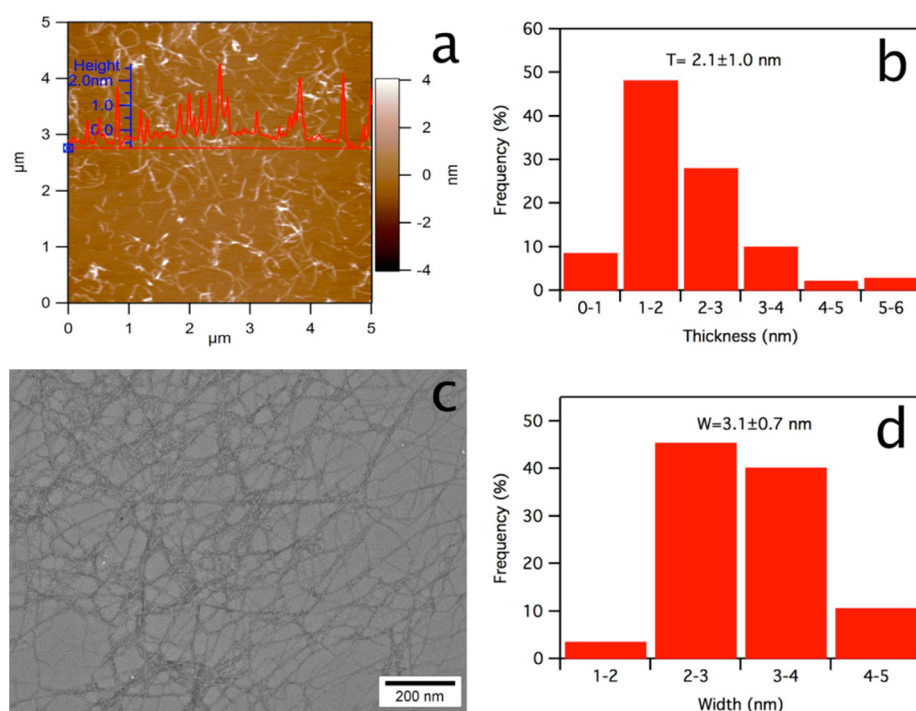
Figure 5. Cellulose nanofibrils from the first hydrolysis at 150 °C: (a) AFM, inset is the height profile along the red line, (b) thickness from AFM, (c) TEM, and (d) width from TEM.

showing consistent HTSACF catalytic activity and persistent cellulose hydrolysis over repeated hydrolysis cycles.

At a lower hydrolysis temperature of 130 °C, nanocellulose was produced at a similar yield of 2.1% but contained more of the shorter CNCs and few longer CNFs (Figure S6b). Hydrolysis at an even lower temperature of 110 °C produced too little nanocellulose to be measured gravimetrically. Similar to sulfonated carbons, solid acid catalysts in biofuel synthesis,[40] or solid metal oxide superacid catalyst in poly(ethylene terphthalate) hydrolysis,[41] the HTSACF-catalyzed hydrolysis is also thought to be through the hydronium ions, whose diffusion and action is affected by both temperature and pressure associated with the hydrothermal conditions. The fact that no nanocellulose was generated at the lower temperature and pressure suggests hydronium ion diffusion and hydrolysis occur primarily on the surface chains to release glucose. At 150 °C, it is postulated that hydronium ions could diffuse faster into the amorphous regions and interspacing between crystallites while simultaneous defibrillation of partially hydrolyzed cellulose into nanofibrils was facilitated by the increased pressure.

Both yields and morphologies of CNFs from hydrolysis catalyzed by HTSACFs at 150 °C were compared with CNCs from sulfuric acid hydrolysis[42] and CNFs from TEMPO oxidation,[33,43] all from the same rice straw cellulose. The 8.1% cumulative yield of CNFs generated from the solid acid HTSACF catalyst was slightly higher than the 6.8% yield of CNCs from sulfuric acid hydrolysis, but the CNFs were only one-half in the lateral dimension (2.1 nm thick and 3.1 nm wide) and much longer (up to 1 μm) than the rigid rodlike CNCs (4.7 nm thick, 6.4 nm wide, and 143 nm long). These CNFs generated from the solid acid HTSACF catalysts were close in lateral dimensions to those of CNFs (1.5 nm thick and 2.0 nm wide) isolated from TEMPO oxidation and mechanical blending. Most significantly, hydrolysis by these solid HTSACF

catalysts produces both CNFs and nearly exclusively glucose, which could be facilely separated from the solid catalyst via dialysis and filtration, respectively. This is in contrast to sulfuric acid hydrolysis, where cellulose was hydrolyzed into a mixture of glucose, oligosaccharides, and/or hydroxymethylfurfural that were inseparable from the liquid acid. In essence, three consecutive hydrolyses by HTSACFs converted 72.1% of cellulose fully into 64% glucose and 8.1% CNF, while the residual cellulose and HTSACFs could be continuously hydrolyzed to generate even more glucose and CNFs with additional repeats.

Formation of primarily longer and narrower CNFs rather than CNCs also indicates a different hydrolysis mechanism by these solid acid catalysts than the strong liquid sulfuric acid. Sulfuric acid diffuses into cellulose through the least ordered amorphous regions and the interspacing between crystallites, cleaving all accessible glycosidic bonds to produce sugar fragments and to release individual cellulose nanocrystals. Not only do these solid HTSACF catalysts have significantly lower acid density (0.88 mmol/g) than the concentrated sulfuric acid (13 mmol/g), the acid sites on the pore surfaces of the HTSACF catalyst do not function by direct access. Instead, the hydronium ions diffuse from HTSACFs into the contacting surface layer of cellulose to cleave the hydrogen bond among amorphous chains and crystallites to peel off thin nanofibrils from the cellulose surface. The fragments from the amorphous and crystallite surface chains could be further hydrolyzed into glucose via acid sites on the predominantly mesoporous HTSACF pore surfaces. The higher pressures associated with increasing temperatures, e.g., 5 atm at 150 °C, may also facilitate the layer-by-layer peeling and defibrillation process, leaving long and thin flexible cellulose nanofibrils.

CONCLUSIONS

One-dimensinoal mesoporous fibrous (500 nm to 2 μm wide, tens of micrometers long) acid catalysts were prepared via direct sulfonation of ultrafine activated carbon fibers derived from lignin to contain 0.56 mmol/g sulfonic and 0.88 mmol/g total acid densities. Direct hydrothermal hydrolysis of highly crystalline rice straw cellulose reached 69.8% extent from three consecutive runs at 91.7% glucose selectively, which is much higher than other solid catalysts reported to date. Meanwhile, cellulose nanofibrils (2.1 nm thick, 3.1 nm wide, and up to 1 μm long) were simultaneously generated at a cumulative 8.1% yield. This exemplifies lignin utilization and cellulose conversion into easily separable glucose for biofuel and high value nanocellulose.

ASSOCIATED CONTENT

Ⓢ Supporting Information

The Supporting Information is available free of charge on the ACS Publications website at DOI: 10.1021/acssusche-meng.5b00780.

> Standard calibration curve for glucose concentration; conductometric titration curves for lignin-based catalyst; illustration of cellulose hydrolysis by HTSACF and liquid acid; LC-MS spectra of the hydrolysate from cellulose hydrolysis; optical microscope images of a cast film from cellulose nanofibrils; and more AFM height images of cellulose nanofibrils (PDF)

AUTHOR INFORMATION

Corresponding Author
*Tel.: +1 530 752 0843. E-mail: ylhsieh@ucdavis.edu.

Notes
The authors declare no competing financial interest.

ACKNOWLEDGMENTS

REFERENCES

(1) Mizuno, N.; Misono, M. Heterogeneous catalysis. *Chem. Rev.* **1998**, *98* (1), 199−218.

(2) Conner, W. C., Jr; Falconer, J. L. Spillover in heterogeneous catalysis. *Chem. Rev.* **1995**, *95* (3), 759−788.

(3) Kiss, A. A.; Dimian, A. C.; Rothenberg, G. Solid acid catalysts for biodiesel production - Towards sustainable energy. *Adv. Synth. Catal.* **2006**, *348* (1−2), 75−81.

(4) Corma, A. Inorganic Solid Acids and Their Use in Acid-Catalyzed Hydrocarbon Reactions. *Chem. Rev.* **1995**, *95* (3), 559−614.

(5) Haw, J. F. Zeolite acid strength and reaction mechanisms in catalysist. *Phys. Chem. Chem. Phys.* **2002**, *4* (22), 5431−5441.

(6) Choudary, B. M.; Sateesh, M.; Kantam, M. L.; Rao, K. K.; Prasad, K. V. R.; Raghavan, K. V.; Sarma, J. A. R. P. Selective nitration of aromatic compounds by solid acid catalysts. *Chem. Commun.* **2000**, No. 1, 25−26.

(7) Lim, M. H.; Blanford, C. F.; Stein, A. Synthesis of ordered microporous silicates with organosulfur surface groups and their applications as solid acid catalysts. *Chem. Mater.* **1998**, *10* (2), 467−470.

(8) Kozhevnikov, I. V.; Sinnema, A.; Jansen, R. J. J.; Pamin, K.; Vanbekkum, H. New Acid Catalyst Comprising Heteropoly Acid on a Mesoporous Molecular-Sieve Mcm-41. *Catal. Lett.* **1995**, *30* (1−4), 241−252.

(9) Van Rhijn, W. M.; De Vos, D. E.; Sels, B. F.; Bossaert, W. D.; Jacobs, P. A. Sulfonic acid functionalised ordered mesoporous materials as catalysts for condensation and esterification reactions. *Chem. Commun.* **1998**, No. 3, 317−318.

(10) Umbarkar, S. B.; Biradar, A. V.; Mathew, S. M.; Shelke, S. B.; Malshe, K. M.; Patil, P. T.; Dagde, S. P.; Niphadkar, S. P.; Dongare, M. K. Vapor phase nitration of benzene using mesoporous MoO3/SiO2 solid acid catalyst. *Green Chem.* **2006**, *8* (5), 488−493.

(11) Harmer, M. A.; Farneth, W. E.; Sun, Q. High surface area nafion resin/silica nanocomposites: A new class of solid acid catalyst. *J. Am. Chem. Soc.* **1996**, *118* (33), 7708−7715.

(12) Kulkarni, M. G.; Gopinath, R.; Meher, L. C.; Dalai, A. K. Solid acid catalyzed biodiesel production by simultaneous esterification and transesterification. *Green Chem.* **2006**, *8* (12), 1056−1062.

(13) Bringue, R.; Tejero, J.; Iborra, M.; Izquierdo, J. F.; Fite, C.; Cunill, F. Supported Nafion catalyst for 1-pentanol dehydration reaction in liquid phase. *Chem. Eng. J.* **2008**, *145* (1), 135−141.

(14) Kaspi, J.; Montgomery, D. D.; Olah, G. A. Heterogeneous Catalysis by Solid Superacids 0.5. Methylation of Benzene and Methylbenzenes with Methyl-Alcohol over a Perfluorinated Resin-sulfonic Acid (Nafion-H) Catalyst. *J. Org. Chem.* **1978**, *43* (16), 3147−3150.

(15) Hegner, J.; Pereira, K. C.; DeBoef, B.; Lucht, B. L. Conversion of cellulose to glucose and levulinic acid via solid-supported acid catalysis. *Tetrahedron Lett.* **2010**, *51* (17), 2356−2358.

(16) Shu, Q.; Zhang, Q.; Xu, G. H.; Nawaz, Z.; Wang, D. Z.; Wang, J. F. Synthesis of biodiesel from cottonseed oil and methanol using a carbon-based solid acid catalyst. *Fuel Process. Technol.* **2009**, *90* (7−8), 1002−1008.

(17) Yamaguchi, D.; Hara, M. Starch saccharification by carbon-based solid acid catalyst. *Solid State Sci.* **2010**, *12* (6), 1018−1023.

(18) Pang, J. F.; Wang, A. Q.; Zheng, M. Y.; Zhang, T. Hydrolysis of cellulose into glucose over carbons sulfonated at elevated temperatures. *Chem. Commun.* **2010**, *46* (37), 6935−6937.

(19) Huang, Y. B.; Fu, Y. Hydrolysis of cellulose to glucose by solid acid catalysts. *Green Chem.* **2013**, *15* (5), 1095−1111.

(20) Cai, H. L.; Li, C. Z.; Wang, A. Q.; Xu, G. L.; Zhang, T. Zeolite-promoted hydrolysis of cellulose in ionic liquid, insight into the mutual behavior of zeolite, cellulose and ionic liquid. *Appl. Catal., B* **2012**, *123*, 333−338.

(21) Lai, D.-m.; Deng, L.; Guo, Q.-x.; Fu, Y. Hydrolysis of biomass by magnetic solid acid. *Energy Environ. Sci.* **2011**, *4* (9), 3552−3557.

(22) Zhang, F.; Deng, X.; Fang, Z.; Tian, X.; Kozinski, J. Hydrolysis of crystalline cellulose over Zn−Ca−Fe oxide catalyst. *Petrochem. Technol.* **2011**, *40*, 43−48.

(23) Toda, M.; Takagaki, A.; Okamura, M.; Kondo, J. N.; Hayashi, S.; Domen, K.; Hara, M. Default green chemistry: biodiesel made with sugar catalyst. *Nature* **2005**, *438*, 178−178.

(24) Kitano, M.; Yamaguchi, D.; Suganuma, S.; Nakajima, K.; Kato, H.; Hayashi, S.; Hara, M. Adsorption-enhanced hydrolysis of β-1, 4-Glucan on graphene-based amorphous carbon bearing SO3H, COOH, and OH groups. *Langmuir* **2009**, *25* (9), 5068−5075.

(25) Fukuhara, K.; Nakajima, K.; Kitano, M.; Kato, H.; Hayashi, S.; Hara, M. Structure and Catalysis of Cellulose-Derived Amorphous Carbon Bearing SO3H Groups. *ChemSusChem* **2011**, *4* (6), 778−784.

(26) Onda, A.; Ochi, T.; Yanagisawa, K. Selective hydrolysis of cellulose into glucose over solid acid catalysts. *Green Chem.* **2008**, *10* (10), 1033−1037.

(27) Guo, H.; Qi, X.; Li, L.; Smith, R. L., Jr Hydrolysis of cellulose over functionalized glucose-derived carbon catalyst in ionic liquid. *Bioresour. Technol.* **2012**, *116*, 355−359.

(28) Suganuma, S.; Nakajima, K.; Kitano, M.; Yamaguchi, D.; Kato, H.; Hayashi, S. Hydrolysis of cellulose by amorphous carbon bearing SO3H, COOH, and OH groups. *J. Am. Chem. Soc.* **2008**, *130* (38), 12787−12793.

(29) Onda, A.; Ochi, T.; Yanagisawa, K. Hydrolysis of cellulose selectively into glucose over sulfonated activated-carbon catalyst under hydrothermal conditions. *Top. Catal.* **2009**, *52* (6−7), 801−807.

(30) Tang, L. R.; Huang, B.; Ou, W.; Chen, X. R.; Chen, Y. D. Manufacture of cellulose nanocrystals by cation exchange resin-

catalyzed hydrolysis of cellulose. *Bioresour. Technol.* **2011**, *102* (23), 10973−10977.

(31) Hu, S.; Hsieh, Y. L. Ultrafine microporous and mesoporous activated carbon fibers from alkali lignin. *J. Mater. Chem. A* **2013**, *1* (37), 11279−11288.

(32) Lu, P.; Hsieh, Y. L. Preparation and characterization of cellulose nanocrystals from rice straw. *Carbohydr. Polym.* **2012**, *87* (1), 564−573.

(33) Jiang, F.; Hsieh, Y.-L. Chemically and mechanically isolated nanocellulose and their self-assembled structures. *Carbohydr. Polym.* **2013**, *95* (1), 32−40.

(34) Mikhail, R. S.; Brunauer, S.; Bodor, E. E. Investigations of a Complete Pore Structure Analysis.I. Analysis of Micropores. *J. Colloid Interface Sci.* **1968**, *26* (1), 45−53.

(35) Harkins, W. D.; Jura, G. An adsorption method for the determination of the area of a solid without the assumption of a molecular area, and the area occupied by nitrogen molecules on the surfaces of solids. *J. Chem. Phys.* **1943**, *11* (9), 431−432.

(36) Miller, G. L. Use of dinitrosalicylic acid reagent for determination of reducing sugar. *Anal. Chem.* **1959**, *31* (3), 426−428.

(37) Hu, S.; Zhang, S.; Pan, N.; Hsieh, Y.-L. High energy density supercapacitors from lignin derived submicron activated carbon fibers in aqueous electrolytes. *J. Power Sources* **2014**, *270*, 106−112.

(38) Groen, J. C.; Peffer, L. A. A.; Perez-Ramirez, J. Pore size determination in modified micro- and mesoporous materials. Pitfalls and limitations in gas adsorption data analysis. *Microporous Mesoporous Mater.* **2003**, *60* (1−3), 1−17.

(39) Ravikovitch, P. I.; Neimark, A. V. Experimental confirmation of different mechanisms of evaporation from ink-bottle type pores: Equilibrium, pore blocking, and cavitation. *Langmuir* **2002**, *18* (25), 9830−9837.

(40) Guo, F.; Fang, Z.; Xu, C. C.; Smith, R. L. Solid acid mediated hydrolysis of biomass for producing biofuels. *Prog. Energy Combust. Sci.* **2012**, *38* (5), 672−690.

(41) Li, X. K.; Lu, H.; Guo, W. Z.; Cao, G. P.; Liu, H. L.; Shi, Y. H. Reaction kinetics and mechanism of catalyzed hydrolysis of waste PET using solid acid catalyst in supercritical CO2. *AIChE J.* **2015**, *61* (1), 200−214.

(42) Jiang, F.; Dallas, J. L.; Ahn, B. K.; Hsieh, Y. L. 1D and 2D NMR of nanocellulose in aqueous colloidal suspensions. *Carbohydr. Polym.* **2014**, *110*, 360−366.

(43) Jiang, F.; Han, S.; Hsieh, Y.-L. Controlled defibrillation of rice straw cellulose and self-assembly of cellulose nanofibrils into highly crystalline fibrous materials. *RSC Adv.* **2013**, *3* (30), 12366−12375.